Boundary-Layer Meteorol (2011) 139:261–281
DOI 10.1007/s10546-010-9583-z

ARTICLE

Intercomparison of Planetary Boundary-Layer Parametrizations in the WRF Model for a Single Day from CASES-99

Hyeyum Hailey Shin · Song-You Hong

Received: 5 June 2010 / Accepted: 22 December 2010 / Published online: 20 January 2011

Abstract This study compares five planetary boundary-layer (PBL) parametrizations in the Weather Research and Forecasting (WRF) numerical model for a single day from the Cooperative Atmosphere-Surface Exchange Study (CASES-99) field program. The five schemes include two first-order closure schemes—the Yonsei University (YSU) PBL and Asymmetric Convective Model version 2 (ACM2), and three turbulent kinetic energy (TKE) closure schemes—the Mellor–Yamada–Janjić (MYJ), quasi-normal scale elimination (QNSE), and Bougeault–Lacarrére (BouLac) PBL. The comparison results reveal that discrepancies among thermodynamic surface variables from different schemes are large at daytime, while the variables converge at nighttime with large deviations from those observed. On the other hand, wind components are more divergent at nighttime with significant biases. Regarding PBL structures, a non-local scheme with the entrainment flux proportional to the surface flux is favourable in unstable conditions. In stable conditions, the local TKE closure schemes show better performance. The sensitivity of simulated variables to surface-layer parametrizations is also investigated to assess relative contributions of the surface-layer parametrizations to typical features of each PBL scheme. In the surface layer, temperature and moisture are more strongly influenced by surface-layer formulations than by PBL mixing algorithms in both convective and stable regimes, while wind speed depends on vertical diffusion formulations in the convective regime. Regarding PBL structures, surface-layer formulations only contribute to near-surface variability and then PBL mean properties, whereas shapes of the profiles are determined by PBL mixing algorithms.

Keywords CASES-99 · Intercomparison · Parametrization · Planetary boundary layer · Surface layer · Weather Research and Forecasting model

H. H. Shin · S.-Y. Hong (✉)
Department of Atmospheric Sciences, College of Science, Yonsei University, Seoul 120-749, Korea
e-mail: shong@yonsei.ac.kr

H. H. Shin
e-mail: hyeyum@yonsei.ac.kr

1 Introduction

Since L. F. Richardson first attempted numerical weather prediction (NWP) in 1922, continuing advancement of human knowledge has been accompanied by increases in computing power. Cutting edge NWP models are typically operated with horizontal resolutions of 10–100 km over the globe. However, the current resolutions are still not fine enough to explicitly resolve all relevant scales of atmospheric motions whose effects must be included in the NWP models to reasonably predict atmospheric states. Turbulent motions belong to these subgrid-scale motions, and can significantly alter the atmospheric status by means of turbulent mixing, predominantly throughout the planetary boundary layer (PBL). This impact of subgrid-scale turbulent motions on grid-scale variables is expressed through PBL parametrizations in atmospheric numerical models.

The importance of PBL parametrizations in numerical prediction has been actively emphasized in recent decades. For weather prediction, Hong and Pan (1996) showed that the prediction skills of a medium-range forecast model in forecasting precipitation are sensitive to the vertical mixing formulation, and to parameters such as the critical Richardson number used for determining the boundary-layer height. Especially for hurricane simulations, Braun and Tao (2000) and Li and Pu (2008) suggested that PBL schemes are as important as cloud-microphysics schemes in forecasting hurricane intensity and accompanying precipitation. As a study on the impact of PBL schemes in seasonal simulations using a general circulation model, Holtslag and Boville (1993) showed an improvement of boundary-layer transport in dry convective conditions by changing the PBL algorithm. Recently, Steeneveld et al. (2008) evaluated the abilities of three regional models in predicting diurnal cycles, with special attention to the stable boundary layer (SBL) in the CASES-99 experimental campaign. They showed that model results are sensitive to the choice of PBL parametrization both at daytime and nighttime, while the simulated results of the nocturnal boundary layer are especially sensitive to the radiation scheme.

The PBL parametrizations implemented in large-scale atmospheric numerical models are largely divided into first-order or one-and-a-half order (TKE) closure schemes. These methods have been evaluated against in situ observations or statistics from large-eddy simulations in previous studies (e.g., Holt and Raman 1988; Musson-Genon 1995; Sharan and Gopalakrishnan 1997; Cuxart et al. 2006; Svensson and Holtslag 2006). Holt and Raman (1988) comparatively evaluated eleven PBL schemes with a one-dimensional barotropic boundary-layer model. They concluded that the simulated mean boundary-layer structure is hardly sensitive to the order of the closure, while the turbulent structure is better represented using the TKE closure. Musson-Genon (1995) found that differences among the different closures occur for cloudy conditions, and the differences mainly occur through varying tunable parameters rather than closure types. Sharan and Gopalakrishnan (1997) revealed that under strong (weak) wind conditions, the profiles of turbulent diffusivities are quite insensitive (sensitive) to PBL parametrizations, but the resultant mean wind and thermodynamic variables are quite variable (invariable) depending on PBL parametrizations. Recently, Cuxart et al. (2006) compared 19 single column models (SCM), used by major operational NWP centres and research groups, for a moderately stratified atmospheric boundary layer using statistics from a corresponding large-eddy simulation intercomparison as references, under the first GEWEX (Global Energy and Water Cycle Experiment) Atmospheric Boundary Layer Study (GABLS) project. Generally, it was seen that the operational models produce stronger mixing, resulting in the omission of the upper inversion development and overestimation of the surface friction velocity. Svensson and Holtslag (2006) documented the intercomparison of 18 SCMs to examine the validity of boundary-layer schemes in current NWP and climate

models under the second GABLS project. These one-dimensional model studies showed that the models produce very divergent results in all compared variables, and there are noticeable discrepancies between the simulated values and observations.

The WRF model has eight PBL schemes, and continuous efforts have been made to investigate the sensitivity of the simulated precipitation and large-scale fields to these PBL schemes. However, there are few studies that document typical characteristics of one scheme compared to others in both unstable and stable boundary-layer regimes, focusing on the main roles of the PBL schemes: prediction of near-surface and PBL properties. In this paper, five PBL parametrizations in the WRF model—the YSU (Yonsei University: YSU, Hong et al. 2006), ACM2 (Asymmetric Convective Model version 2: ACM2, Pleim 2007b), MYJ (Mellor–Yamada–Janjić: MYJ, Janjić 1990), QNSE (quasi-normal scale elimination: QNSE, Sukoriansky et al. 2005), and BouLac (Bougeault–Lacarrére: BouLac, Bougeault and Lacarrére 1989) PBL—are compared for one day from the CASES-99 field program. The objective of the study is to compare characteristic features of each PBL parametrization, and from the intercomparison we aim to examine the advantages and disadvantages of different approaches, and to identify the characteristics that need to be considered for the future improvement of PBL schemes. Furthermore, the sensitivity of the performance of a PBL parametrization to surface-layer formulations is also investigated. Since each PBL scheme is tied to particular surface-layer schemes in the WRF model, we aim to assess the relative contribution of surface-layer formulations to the typical behaviour of PBL parametrizations by conducting the sensitivity experiments to surface-layer schemes. Note that previous studies investigating the sensitivity of WRF simulations to the choice of PBL scheme did not assess the relative contribution of the surface-layer schemes, even though the surface-layer formulations are different in the various PBL schemes used.

A brief review of PBL and surface-layer parametrizations is provided in Sect. 2, and Sect. 3 presents a case description. Experimental design for the intercomparison of PBL parametrizations and surface-layer sensitivity simulations is given in Sect. 4, and results are given in Sect. 5. Concluding remarks follow in the final section.

2 A Brief Review of PBL and Surface-Layer Parametrizations

2.1 PBL Parametrizations

In PBL parametrizations, subgrid-scale turbulent fluxes are parameterized using prognostic mean variables (C; u, v, θ, q), through vertical diffusion equations. The simplest relation for the vertical diffusion can be expressed as

$$\frac{\partial C}{\partial t} = -\frac{\partial}{\partial z}\overline{w'c'} = \frac{\partial}{\partial z}\left[K_c\left(\frac{\partial C}{\partial z}\right)\right] \tag{1}$$

where K_c is the diffusivity for the mean variable C.

First-order closure—the YSU and ACM2 PBL schemes

The YSU (Hong et al. 2006) and ACM2 (Pleim 2007b) PBL schemes are classified as first-order closure schemes, since they do not require any additional prognostic equations to express the effects of turbulence on mean variables. For the convective boundary layer (CBL), both schemes are based on the K profile in determining the diffusivity K_c within the boundary layer (hereafter, $K_{profile}$), while K_c is a function of local wind shear and local Richardson number (K_{local}) in the free atmosphere.

In addition to the simple local diffusion in (1), both the YSU and ACM2 PBL schemes consider non-local mixing by convective large eddies. The YSU scheme expresses the non-local mixing by simply adding a non-local gradient adjustment term (γ_c) to the local gradient of each prognostic mean variable for heat and momentum components:

$$\frac{\partial C}{\partial t} = \frac{\partial}{\partial z}\left[K_c\left(\frac{\partial C}{\partial z} - \gamma_c\right) - \overline{(w'c')}_h\left(\frac{z}{h}\right)^3\right], \tag{2}$$

though the YSU does not employ the gradient adjustment term to passive scalars (e.g., q_v). One of the major ingredients of the YSU algorithm is the explicit treatment of entrainment processes at the top of the PBL; at the inversion layer an asymptotic entrainment flux term proportional to the surface flux is included (i.e., the last term of the right-hand side in Eq. 2) (see Noh et al. 2003 for further details). For SBL, the local scheme in which the mixing coefficient is a function of the local Richardson number at a given model level (Hong et al. 2006) is replaced by an enhanced diffusion of Hong (2010), which is based on the bulk Richardson number between the surface layer and the top of the boundary layer.

For prognostic mean variables at layer i, the ACM2 scheme explicitly contains non-local upward fluxes from the surface and downward fluxes from (to) the adjacent upper (lower) vertical level (i.e., the first, second, and third terms of the right-hand side in Eq. 3), for heat, moisture, and momentum components:

$$\begin{aligned}\frac{\partial C_i}{\partial t} &= f_{conv} Mu C_1 - f_{conv} Md_i C_i + f_{conv} Md_{i+1} C_{i+1}\frac{\Delta z_{i+1}}{\Delta z_i} \\ &+ \frac{\partial}{\partial z}\left(K_c\left(1 - f_{conv}\right)\frac{\partial C}{\partial z}\right),\end{aligned} \tag{3}$$

where Mu is the non-local upward convective mixing rate (s^{-1}) from the top of the lowest model layer, Md_i is the non-local downward mixing rate from layer i to $i-1$, Δz_i is the layer thickness, and f_{conv} is the critical factor that determines the ratio of the contribution of the non-local mixing to the total mixing. Pleim (2007a) showed that the local component (i.e., the eddy-diffusion term in Eq. 3) is responsible for most of the negative (downward) heat fluxes in the entrainment zone. In the ACM2 scheme, maximum of the $K_{profile}$ and K_{local} is used as K_c of the eddy-diffusion term in Eq. 3, under unstable conditions within the PBL (Pleim 2007b). Thus, the negative entrainment flux is considered as the local flux with K_{local}, since $K_{profile}$ approaches zero near h. For SBL, the local mixing scheme with K_{local} is used.

TKE closure—the MYJ, QNSE, and BouLac PBL schemes

The MYJ, QNSE, and BouLac PBL schemes are classified as TKE closure (one-and-a-half order closure) schemes, requiring one additional prognostic equation of the TKE (i.e., e). In the three TKE closure schemes, the diffusivity in (1) is commonly expressed as

$$K_c = l\sqrt{e}S_c, \tag{4}$$

where l is the mixing length, and S_c is the proportional coefficient. The three TKE closure schemes differ in how they define S_c and l. Three local TKE closure schemes apply the local mixing with the local diffusivity (4) from the lowest to the highest vertical level for both CBL and SBL, and there is no separation between the PBL and the free atmosphere mixing. Thus, the entrainment is represented using the computed K_c from the prognostic TKE near the PBL top.

These three parametrization methods are explained in more detail in Janjić (1990) (MYJ), Sukoriansky et al. (2005) (QNSE), and Bougeault and Lacarrére (1989) (BouLac). Note that

the QNSE PBL scheme employs the diffusivity obtained from the spectral theory to reflect effects of internal wave generation in the presence of turbulence in the stably stratified boundary layer. The vertical scalar mixing is totally suppressed by the stable stratification, whereas vertical momentum mixing continues even at low Froude numbers (*Fr*) (Sukoriansky et al. 2005). The QNSE theory is valid for stable stratification and weakly unstable conditions, while improvement for the unstable case is in progress (Galperin and Sukoriansky 2010).

2.2 Surface-Layer Parametrizations

The role of surface-layer parametrizations in atmospheric numerical models is to calculate the surface exchange coefficients (C_D and C_H) to compute the sensible and latent heat fluxes, and momentum flux, consistent with the flux–profile relationships. Currently, each PBL parametrization is tied to particular surface-layer schemes in the WRF model, except for the BouLac PBL scheme. The surface-layer schemes tied to each PBL parametrization are: the MM5 surface-layer similarity (Zhang and Anthes 1982) and the YSU PBL, the PX surface-layer similarity (Pleim 2006) and the ACM2 PBL, the Eta surface-layer similarity (Janjić 1990) and the MYJ PBL, and the QNSE surface-layer similarity consistent with the QNSE theory (Sukoriansky et al. 2005; Galperin and Sukoriansky 2010) and the QNSE PBL (Skamarock et al. 2008). The Eta similarity is also used for the BouLac experiment.

The fluxes are calculated as:

$$\tau_0 = -\rho\overline{U'w'}_s = \rho K_M \frac{\partial U}{\partial z} = \rho u_*^2 = \rho C_D U_1^2, \tag{5}$$

$$H_0 = \rho c_p \overline{\theta'w'}_s = -\rho c_p K_H \frac{\partial \theta}{\partial z} = -\rho c_p u_* \theta_* = -\rho c_p C_H U_1(\theta_1 - \theta_s), \tag{6}$$

$$LH = \rho L_v \overline{q'w'}_s = -\rho L_v K_H \frac{\partial q}{\partial z} = -\rho L_v u_* q_* = -\rho L_v C_H U_1(q_1 - q_s). \tag{7}$$

Here, the subscripts '1' and 's' designate the value at the lowest model-layer height (z_1) and surface, respectively. These fluxes are provided as lower boundary conditions in all PBL schemes. The 2-m temperature and 10-m wind speed are also diagnosed, and are interpolated between z_1 and the surface using the flux–profile relationship (i.e., consistent with the surface-layer formulation).

3 A Case Description

In our study, five PBL schemes are compared for one day from the CASES-99 field experimental campaign, for 24 h from 1200 UTC 23 October to 1200 UTC 24 October 1999. The CASES-99 field program was held during the month of October 1999 in Leon, Kansas, U.S.A. (Poulos et al. 2002). The main site was located at 96.7°W, 37.6°N. The location is relatively flat and covered by grassland, and it was under a clear sky and dry environment during the 24-h period of interest.

Synoptic fields at 850-hPa level are obtained every 12 h from the National Centers for Environmental Prediction (NCEP) final analysis (FNL) data (Fig. 1). At 1200 UTC 23 October (Fig. 1a), an anticyclone is located over the western United States, with the highest geopotential height over the Texas Panhandle. This system is associated with northerly winds over the CASES-99 main site, with wind speeds of roughly 20 m s^{-1}. The relative humidity at the site is approximately 30%. After 12 h, the anticyclone moves further south-eastward,

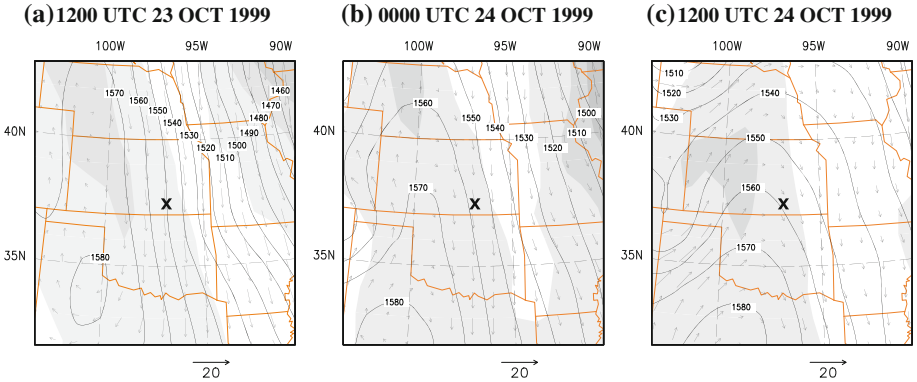

Fig. 1 Analyzed 850-hPa synoptic fields of geopotential heights (m) (*black solid*), winds ($m\,s^{-1}$) (*grey arrows*), and relative humidity (%) (*shaded*) from the National Centers for Environmental Prediction (NCEP) final analysis (FNL) data at **a** 1200 UTC 23 October, **b** 0000 UTC 24 October, and **c** 1200 UTC 24 October 1999. The relative humidity is shaded every 20%. *Cross marks* indicate the CASES-99 main site

so that the ridge is located west of the main site at 0000 UTC 24 October (Fig. 1b). Due to the approaching anticyclone, the lower atmosphere at the main site experiences wind speeds of approximately $10\,m\,s^{-1}$, and less humid conditions. After 12 h at 1200 UTC 24 October (Fig. 1c), the 850-hPa ridge is located over the main site, and the synoptic forcing is weak with wind speeds of $5\,m\,s^{-1}$. Due to the passage of the anticyclone, the wind speed and the amount of moisture decrease in the PBL over the main site during the 24 h. The radiosonde soundings showed that the PBL-averaged wind speed decreases from about 18 to $8\,m\,s^{-1}$, and the specific humidity also decreases below 1,000 m (not shown).

As references for the intercomparison, surface measurements are provided from six 10-m towers surrounding the centre of the main site at 96.7°W, 37.6°N, and vertical profiles are obtained from radiosonde soundings that were made at Leon (96.4°W, 37.4°N, 436 m above the ground) (http://www.eol.ucar.edu/isf/projects/cases99/). It is noted that the simulation period accounts for one complete diurnal cycle of the GABLS2 intercomparison project (Svensson and Holtslag 2006).

4 Experimental Design

The Advanced Research WRF (ARW) numerical model version 3.2 is adopted, which is constructed based on a fully compressible and nonhydrostatic dynamic core. The model uses terrain-following hydrostatic pressure for the vertical coordinate. The model performs reasonably well for detailed NWP cases with real-data initial and boundary conditions.

The model configuration consists of a parent domain and two nested domains centred on the location of the CASES-99 main site (96.7°W, 37.6°N) in the Lambert conformal space (Fig. 2). A 3-km resolution domain (Do3, 49×49) is nested inside a 9-km resolution domain (Do2, 49×49), and the 9-km resolution domain is nested inside a 27-km resolution domain (Do1, 49×49) using a one-way interaction method such that only coarse grid results give their forecast information to finer grid results, and not vice versa. The vertical grid system consists of 28 full-σ levels, and the model top is located at 50 hPa. Under this vertical resolution, there are nine layers below 2,000 m. The lowest full-σ level above the ground is 0.990 ($\sigma_2 = 0.990$), and the lowest half-σ level height (z_1) is approximately 40 m (cf. Fig. 3), as

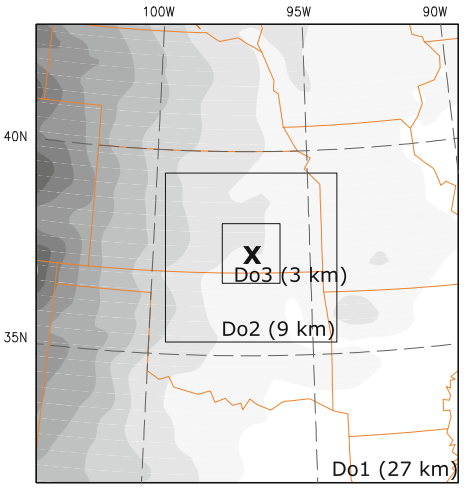

Fig. 2 Model domain for the 27-km resolution experiment (Do1) with terrain heights contoured every 200 m. The *two inner boxes* represent domains for the 9-km (Do2) and 3-km (Do3) resolution experiments, respectively. The *cross* indicates the CASES-99 site

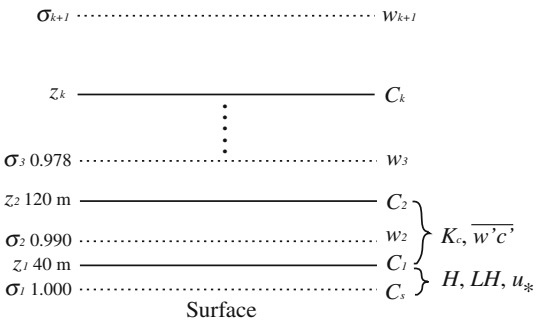

Fig. 3 A schematic diagram illustrating the vertically staggered grid system of the WRF model with specific values in the case of this study. *Dotted* and *solid lines* indicate full-σ and half-σ levels, respectively

in many regional model simulations. These are the default vertical grid-system settings of the WRF model. In the vertically staggered grid system of the WRF model (Fig. 3), the 28 full-σ levels are vertical layer interfaces, and the 27 half-σ levels are responsible for mean states of the vertical layers. The prognostic mean variables (C) are assigned at the half levels, while the vertical velocity (w), diffusivities (K_c), and turbulent fluxes ($\overline{w'c'}$) are assigned at the full levels. In the case of the lowest half-σ level (i.e., z_1) and the surface full-σ level (i.e. $\sigma_1 = 1.0$), surface fluxes are calculated as bulk properties between the surface and z_1; the z_1 is considered to be the surface-layer height in the surface-layer and PBL parametrizations.

Initial and boundary conditions are provided by the NCEP FNL data on $1^\circ \times 1^\circ$ grids, and the boundary conditions are forced every 12 h; in October 1999, the FNL data are only available at 0000 UTC and 1200 UTC. It is noted that the 12-h FNL data produce more realistic simulations than the 6-h NCEP-Department of Energy (DOE) Reanalysis II data in this simulation case (not shown). The model integration is conducted for 24 h from 1200 UTC 23 October (0700 LST 23 October) to 1200 UTC 24 October 1999.

The physics package includes the RRTMG (Rapid Radiative Transfer Model for GCMs) (Mlawer et al. 1997) longwave radiation and Goddard (Chou and Suarez 1999) shortwave radiation processes, as well as the Noah land-surface model (LSM) (Chen and Dudhia 2001; Ek et al. 2003). The land-surface parameters, including the surface moisture availability (M) and roughness length (z_0), are provided according to the U. S. Geological Survey land-use category, with the CASES-99 main site classified as grassland. The moisture availability of

Table 1 A summary of numerical experiments for (a) the intercomparison of PBL parametrizations, and (b) analyses of the sensitivity of a PBL parametrization to surface-layer formulations

Experiment	PBL scheme	Surface-layer scheme
(a)		
YSU	YSU PBL	MM5 similarity
ACM2	ACM2 PBL	PX similarity
MYJ	MYJ PBL	Eta similarity
QNSE	QNSE PBL	QNSE similarity
BouLac	BouLac PBL	Eta similarity
(b)		
BL_YSU	BouLac PBL	MM5 similarity
BL_ACM2	–	PX similarity
BL_MYJ (=BouLac)	–	Eta similarity
BL_QNSE	–	QNSE similarity

"–" in (b) denotes the same scheme with that in the BL_YSU experiment

0.08 and roughness length of 0.03 m are assigned for the grassland category following local observations, as in Steeneveld et al. (2008).

Five simulations with five PBL schemes and their relevant surface-layer schemes are conducted (cf. Sect. 2.2): the YSU PBL and ACM2 PBL of the first-order closure schemes, and the MYJ PBL, QNSE PBL, and BouLac PBL of the TKE closure schemes. The experiments with these PBL schemes are designated as the YSU, ACM2, MYJ, QNSE, and BouLac experiments, respectively. The numerical experiments for the intercomparison of PBL parametrizations are summarized in Table 1a.

The BouLac PBL parametrization is flexible in selecting the surface-layer scheme, thus all surface-layer schemes are available for the BouLac PBL in the current version of the WRF model. Therefore with the BouLac PBL, four experiments with four different surface-layer formulations are conducted to examine the extent to which the intercomparison characteristics of the PBL parametrizations are controlled by the surface-layer options: the BL_YSU with the MM5 surface layer, the BL_ACM2 with the PX surface layer, the BL_MYJ with the Eta surface layer, and the BL_QNSE with the QNSE surface layer (Table 1b).

5 Results

5.1 Surface Variables

Figure 4 shows simulated surface variables from the five intercomparison experiments—the YSU, ACM2, MYJ, QNSE, and BouLac experiments—and corresponding observations. During the daytime heating period up to 1900 UTC (1400 LST), the evolutions of the surface temperatures from the MYJ and BouLac experiments nearly follow those of the observations; the YSU and ACM2 experiments produce warmer surfaces by approximately 3.5 K and 1 K each, while the QNSE experiment underestimates it by about 2.5 K (Fig. 4a). Different from the surface temperature, the model-produced near-surface temperature (i.e., the 2-m temperature) is closest to observations in the YSU experiment (Fig. 4b). However, the temperature from the YSU experiment still keeps increasing at 1900 UTC, when observations and other experiments decrease. The ACM2 experiment shows even warmer air by

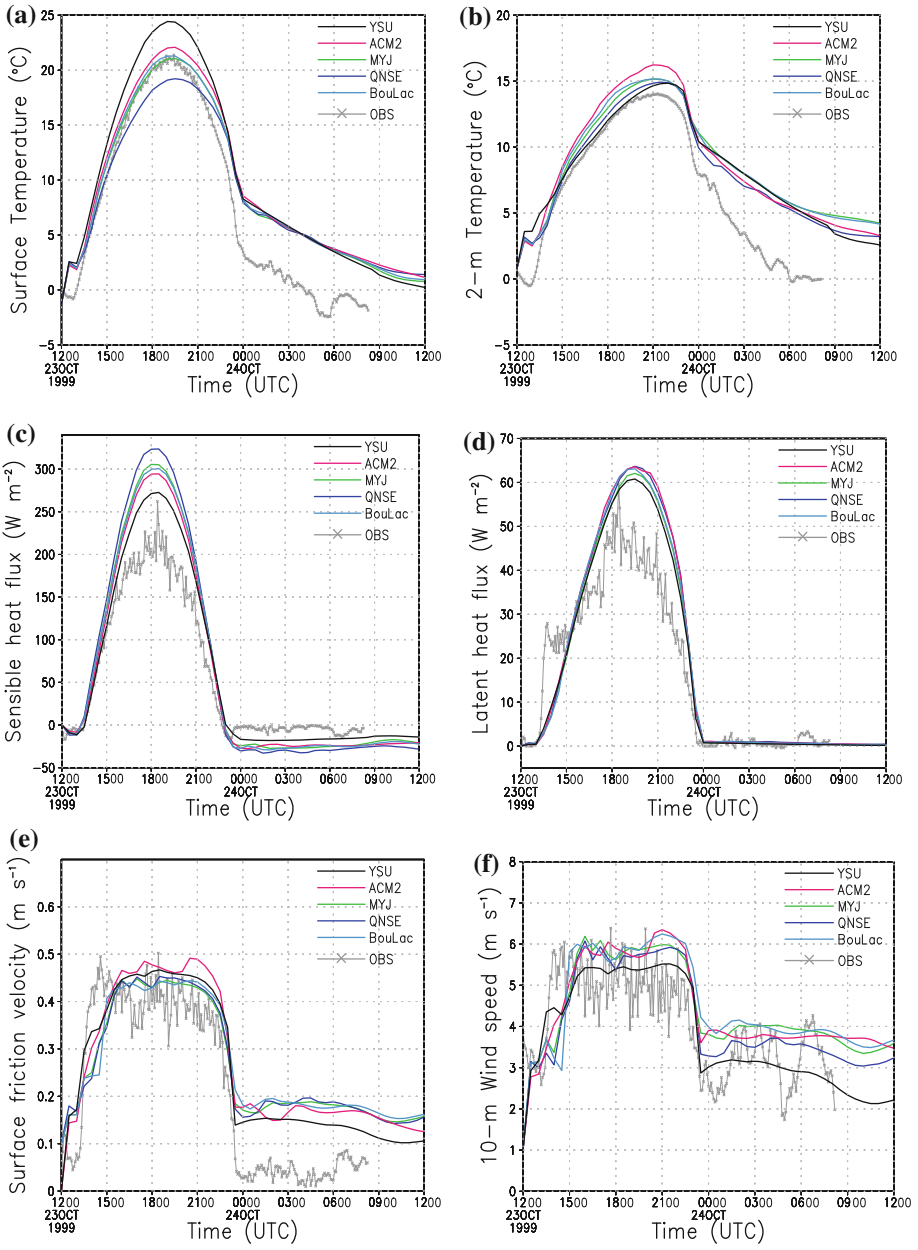

Fig. 4 Time series of simulated **a** surface temperature (°C), **b** 2-m temperature (°C), **c** sensible heat flux ($W\,m^{-2}$), **d** latent heat flux ($W\,m^{-2}$), **e** surface friction velocity ($m\,s^{-1}$), and **f** 10-m wind speed ($m\,s^{-1}$) with corresponding observations (*grey lines with cross marks*). The simulated results are from the YSU (*black*), ACM2 (*red*), MYJ (*green*), QNSE (*blue*), and BouLac (*light blue*) experiments

about 2.5 K than the observed. Therefore, during the daytime the temperature gradient near the surface is largest in the YSU, and it is smallest in the QNSE. During the nighttime, the surface temperature from the YSU experiment tends towards the other four experiments. In other

words, the four experiments underestimate the surface cooling rate during the PBL collapse, as well as during the nighttime. Even though the simulated surface and 2-m temperatures from all the experiments converge at the nighttime, they show positive biases.

Daytime sensible heat fluxes (H) (Fig. 4c) show that the YSU (QNSE) experiment produces the smallest (largest) sensible heat flux. This is opposite to the aforementioned temperature gradient in the daytime. In the Noah LSM, the sensible heat flux is calculated as:

$$H = \rho c_p C_H U_1 (\theta_s - \theta_1), \tag{8}$$

where ρ is the air density, c_p is the specific heat of air at constant pressure, C_H is the surface heat exchange coefficient provided by the surface-layer schemes, U_1 is the wind speed at z_1, and θ_s and θ_1 are the potential temperatures at the surface and z_1, respectively. Thus, it is implied that the surface-layer scheme tied to the YSU (QNSE) PBL parametrization calculates the smallest (largest) C_H, and that the simulated H is not consistent with the near-surface temperature gradient. In other words, the modelled H is more dependent on C_H, and therefore on the surface-layer parametrization, rather than on the temperature gradient near the surface (i.e., on the PBL scheme). The nighttime sensible heat flux is also smallest in the YSU experiment. The latent heat flux is overestimated during the daytime regardless of the PBL scheme, but with negligible differences during the nighttime (Fig. 4d).

The simulated surface friction velocity, u_*, from all experiments lies within the variations of the observations at the daytime, while being overestimated at nighttime (Fig. 4e). The daytime surface friction velocity is largest in the ACM2 experiment, while the three TKE closure experiments simulate the smallest u_*. This order of magnitude of u_* is consistent with the order of magnitude of the mixed-layer wind speed. During the nighttime, the order of magnitude of u_* (i.e., the high u_* in the three TKE closure experiments and the low u_* in the YSU experiment) coincides with the order of magnitude of near-surface wind gradient. The 10-m wind speeds (U_{10}) from the ACM2, MYJ, QNSE, and BouLac experiments are close to the upper value of the observation range, and U_{10} from the YSU experiment is smaller than that from the other four experiments (Fig. 4f). This slight overestimation in all experiments is consistent with preliminary results of the GABLS2 intercomparison project by Svensson and Holtslag (2006); all SCMs reproduce higher 10-m wind speeds than the observations. As mentioned by Svensson and Holtslag (2006), none of the PBL parametrizations can simulate the abrupt increase in the wind speed following the convective initiation in the morning. It is, however, apparent that the YSU and ACM2 experiments that consider non-local momentum mixing simulate more rapid increases of U_{10} in the early stage of mixed-layer development than the three local TKE closure experiments.

Determining the PBL height (h) is important in atmospheric numerical models, because h is used in other physics parametrizations where required (e.g. for the interaction between the orography-induced gravity wave drag and PBL parametrizations revealed by Kim and Hong (2009)). Note that the h-computation methods are not coherent among the five PBL schemes. In the YSU scheme for unstable conditions, the height is determined to be the first neutral level by checking the bulk Richardson number calculated between the lowest model level (z_1) and the levels above (Hong et al. 2006). In the ACM2 scheme, the method is similar to that of the YSU scheme; h is diagnosed as the height above the level of neutral buoyancy where the bulk Richardson number for the entrainment layer exceeds the critical value (Pleim 2007b). Diffusivity profiles are limited below $z = h$ in both schemes, due to the prescribed K profiles (e.g., Eq. (A1) in Hong et al. (2006) and Eq. 1 in Pleim (2007b)). Thus, h and temperature profiles are directly connected in these two K-profile schemes. Meanwhile, in the MYJ, QNSE, and BouLac experiments, h is diagnosed as the height where the prognostic TKE reaches a sufficiently small value (in the current version of the WRF model, the value

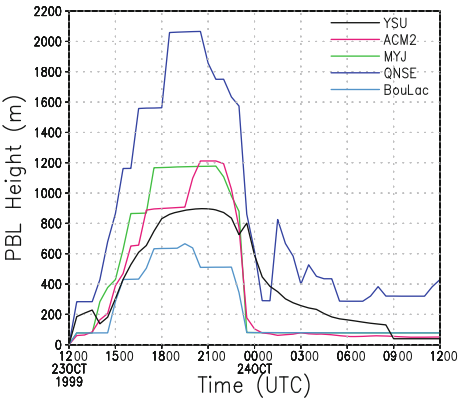

Fig. 5 Time series of the PBL height (m) from five experiments: the YSU (*black*), ACM2 (*red*), MYJ (*green*), QNSE (*blue*), and BouLac (*light blue*) experiments. It is noted that each PBL parametrization uses its own method to diagnose the PBL height, thus, diagnosing methods are not unified

is $0.005\,\mathrm{m^2\,s^{-2}}$). Thus, there is no direct connection between h and the temperature profiles. Since the h-calculation method in a particular PBL scheme is a characteristic of the scheme, we compare h from the five experiments. The calculated PBL heights greatly diverge both during the daytime and the nighttime, with the QNSE PBL scheme calculating the deepest PBL, and the BouLac scheme the shallowest (Fig. 5).

In summary, the thermodynamic variables simulated with the five PBL parametrizations are divergent at daytime, and mean values of the variables from the five simulations are close to the observations. The variables are convergent at nighttime, but the mean values are far from the observations. Unlike the thermal variables, the spreads of simulated u_* and U_{10} are larger at nighttime, with distinct deviations from the tower measurements. These results suggest that the representation of surface variables is still uncertain even using the state-of-the-art PBL schemes, especially under stable conditions. There is no particularly outstanding algorithm.

5.2 PBL Structures

In Fig. 6, K_M (vertical diffusivity for momentum), K_H (vertical diffusivity for heat and moisture), and Pr (Prandtl number) from the five experiments are depicted, which are averaged over both unstable and stable regimes. In the ACM2 scheme K_c multiplied by $(1 - f_{conv})$ is used to express local mixing (cf. Eq. 3), thus depicted in Fig. 6 are the diffusivities $K_c(1 - f_{conv})$. In the convective regime, K_M from the all five experiments shows its maximum at 370 m above the ground but with different magnitudes (Fig. 6a). The diffusivity-profiles from the YSU and ACM2 experiments are similar. However, the ACM2 experiment shows a deeper mixing than the YSU experiment, since the diffusivity of the ACM2 scheme is not zero at h due to the use of K_{local} at h (cf. Sect. 2.1). K_H profiles are designed to be the same as K_M profiles in the ACM2 and BouLac PBL schemes (i.e., $Pr = 1$), while K_H is larger than K_M in the YSU, MYJ, and QNSE PBL schemes (Fig. 6b). Continuous increases of Pr are observed in the YSU and QNSE experiments, while only Pr from the YSU experiment approaches a typical value for weak stratification ($Pr \approx 1$) near the top of the PBL (Fig. 6c).

In the stable regime (Fig. 6d), maximum K_M occurs at different heights with different magnitudes. K_M is very large in the YSU experiment especially below 800 m, due to a parabolic profile function for the diffusion coefficients, but with smaller K_H (Fig. 6e). K_H is about twice as large as K_M in the QNSE experiment. It is necessary to mention that the diffusivities of the YSU and ACM2 experiments increase with height above the top of the

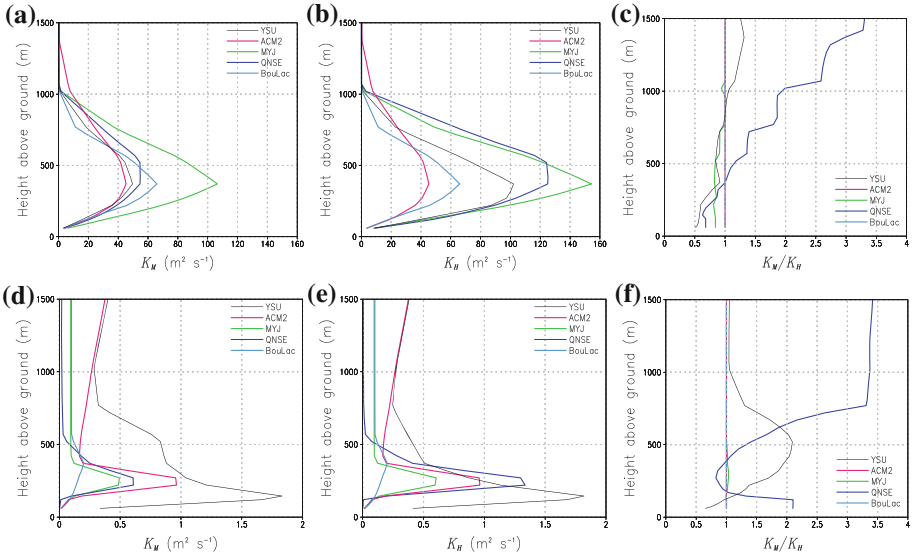

Fig. 6 Eddy viscosity K_M ($m^2\,s^{-1}$) (*left panels*), eddy diffusivity K_H ($m^2\,s^{-1}$) (*centre panels*), and Prandtl number (i.e., K_M/K_H) (*right panels*) **a–c** averaged over 12 h from 1200 UTC 23 October (0700 LST 23 October) to 0000 UTC 24 October (1900 LST 23 October) (i.e., convective regime), and **d–f** averaged over 12 h from 0000 UTC 24 October (1900 LST 23 October) to 1200 UTC 24 October (0700 LST 24 October) (i.e., stable regime)

SBL, where turbulent activities are generally absent. This is due to background diffusivities in these two schemes; the background diffusivity (i.e., K_0) is $0.001\Delta z\ m^2\,s^{-1}$. K_0 values are constant and equal to $0.001\ m^2\,s^{-1}$ and $0.1\ m^2\,s^{-1}$ in the QNSE and BouLac schemes, respectively. In the MYJ scheme, there is no background diffusivity. With respect to Pr (Fig. 6f), it is apparent that $Pr \approx 1$ in the MYJ experiment. The YSU experiment shows a parabolic shape of Pr from 0.5 near the ground and 1 above 500 m, whereas it has a minimum at 300 m in the QNSE experiment. Sukoriansky et al. (2005) showed that Pr^{-1} from the QNSE theory decreases according to increasing stability, since momentum mixing is maintained even in very stable conditions.

The simulated potential temperature, vapour mixing ratio, and wind profiles corresponding to sounding measurements at 1900 UTC 23 October (1400 LST 23 October) are presented in Fig. 7. All PBL parametrizations simulate a warmer and drier PBL than that observed. The observed potential temperature profile is weakly stable in the CBL (Fig. 7a). The YSU experiment forecasts the stable profile well, the ACM2 experiment produces a neutral profile, and the θ profiles are quite unstable in the three TKE experiments. Note that Holtslag and Boville (1993) and Hong and Pan (1996) mentioned that a non-local scheme can produce significant transport for heat while maintaining slightly sub-adiabatic temperature profiles, whereas the upward transport of heat can only occur for absolutely unstable profiles in a local diffusion approach.

The discrepancy between the θ profiles of the YSU and ACM2 experiments is attributed to differences in non-local mixing and entrainment formulations, in addition to the definition of h. In the case of the YSU scheme, the entrainment flux directly related to the surface fluxes would cause stabilization of the mixed layer. This is because the non-local counter-gradient mixing in the scheme is relatively small, but still plays a role in neutralizing the profile

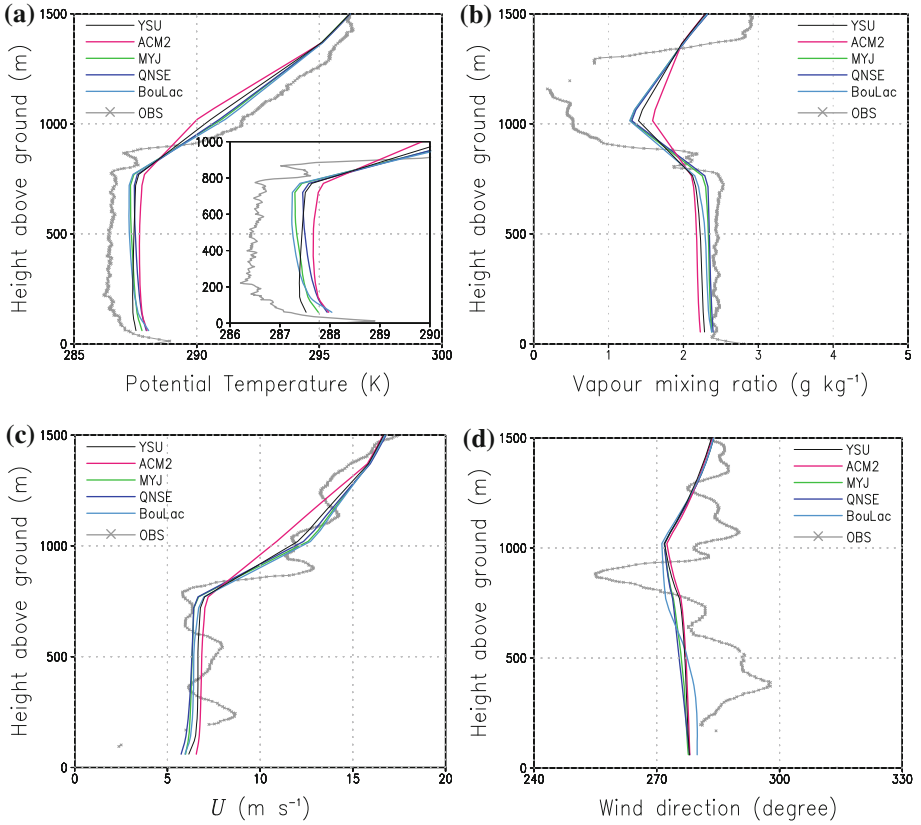

Fig. 7 Vertical profiles of the **a** simulated potential temperature (K), **b** vapour mixing ratio ($g\,kg^{-1}$), **c** wind speed ($m\,s^{-1}$), and **d** wind direction (°) at 1900 UTC 23 October (1400 LST 23 October) with corresponding radiosonde soundings (*grey lines with cross marks*). The simulated results are from the YSU (*black*), ACM2 (*red*), MYJ (*green*), QNSE (*blue*), and BouLac (*light blue*) experiments. In *a*, the *inset* provides a closer look at the temperature profiles in the lowest 1,000 m

(see Fig. 7a of Hong et al. 2006). On the other hand, in the ACM2 scheme the non-local mixing component has a role in increasing the stability of the lowest two thirds of the CBL and lowering the PBL height, whereas the local mixing component with K_{local} contributes to the downward heat fluxes in the entrainment zone (refer to Fig. 8 and explanations of Pleim (2007a)). The ACM2 experiment shows an unexpected bulge in the inversion layer; the bulge appears at the height above h at 1900 UTC 23 October (h is about 900 m at the time), therefore K_H is calculated using K_{local} instead of $K_{profile}$. Thus, the bulge implies that K_{local} of the ACM2 experiment in the inversion layer is too large in this simulation case. It is worth observing discrepancies between the PBL heights and θ profiles in three TKE closure experiments (cp. Figs. 5 and 7a); this is because h is calculated based on the TKE profiles, rather than on the θ profiles as explained in the previous section. The simulated q_v profiles show that the moisture mixing reaches to a higher height of approximately 1,300 m in the ACM2 experiment (Fig. 7b), and this is also closely linked with the large K_{local}.

For wind profiles (Fig. 7c, d) none of the schemes can reproduce a sharp vertical increase of the near-surface wind and fluctuations in the mixed layer. The observation profiles contain

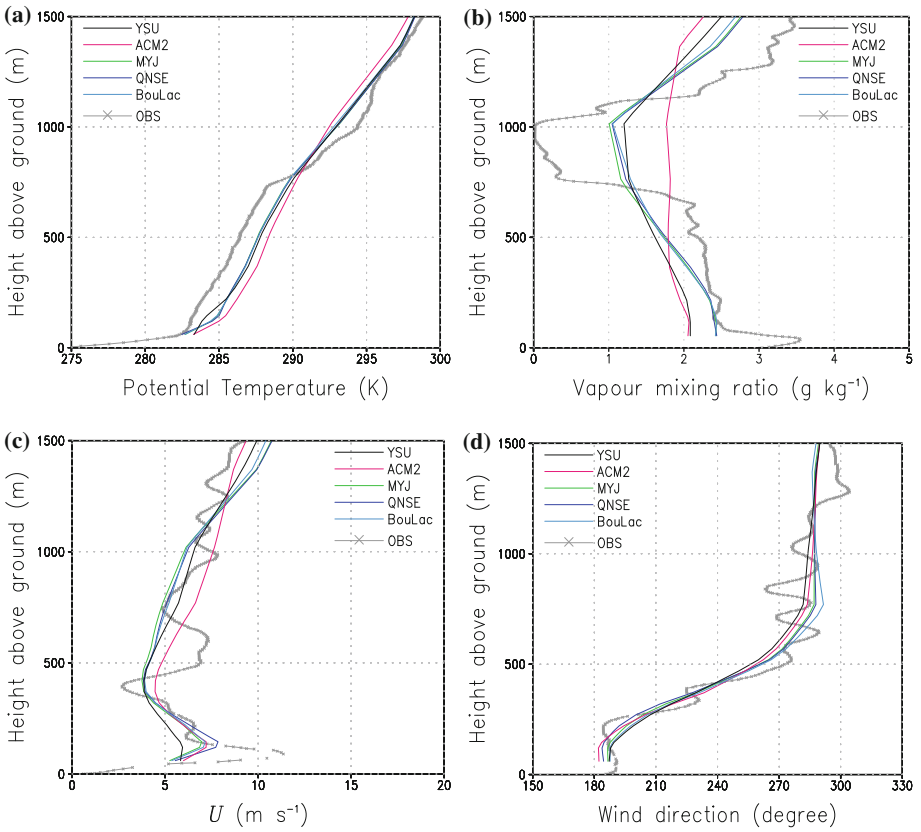

Fig. 8 As in Fig. 7, but at 0700 UTC 24 October (0200 LST 24 October)

turbulent activities that are not averaged out, while PBL schemes express effects of subgrid-scale turbulent fluxes to mean variables, disabling the representation of the observed variability. However, all experiments estimate the average state of the CBL, with wind speed about 6.5 m s^{-1} and reasonable mean wind direction. The two non-local K-profile experiments show slightly stronger winds than the three TKE closure experiments at this time.

Figure 8 compares the simulated vertical profiles of the SBL at 0700 UTC 24 October (0200 LST 24 October). Before 0700 UTC 24 October, the CASES-99 main site experienced weak winds of 5–7 m s^{-1} (cf. Fig. 1). Wiel et al. (2003) classified the night as an intermittent night, when turbulence in the SBL was weak and intermittent (cf. observed H and u_* in Fig. 4). Thus, due to the weak thermal advection and intermittent turbulence, the higher temperatures of the CBL remained at night, except near the surface where strong radiative cooling occurred. Thus, the potential temperature between 100 and 1,000 m showed a weakly stratified PBL (not shown). However, according to the development of the low-level jet (LLJ) near 100 m, shear-driven turbulent mixing occurred, while the strong radiative cooling continued. Thus, the stable layer between 100 and 1,000 m appeared at 0700 UTC 24 October (Fig. 8a).

It is shown that all experiments commonly overestimate SBL temperatures and underestimate the stability of the inversion layer. These common problems occur for two reasons:

overestimation of the surface and near-surface temperatures (i.e., underestimated surface cooling), and underestimation of the LLJ (i.e., underestimated shear-driven turbulence) in all five experiments. Variability of the simulated θ profiles among the five experiments is not notable during the nighttime, except for the YSU and ACM2 experiments. The profile is too-mixed in the YSU experiment near the surface due to the large K_H (cf. Fig. 6e). The ACM2 experiment shows too-mixed θ, q_v, and U profiles above the SBL, especially for water vapour (Fig. 8b). However, both K_M and K_H of the ACM2 experiment have values between the variations of K_M and K_H of the other four experiments (cf. Figs. 6d, e), and θ, q_v, and U profiles are not significantly different from the other experiments below the SBL top. Therefore, the strongly mixed vertical profiles from the ACM2 experiment in the residual layer are mainly attributed to the excessive mixing at the daytime, not to the local nighttime mixing.

With respect to wind profiles (Fig. 8c), it is apparent that all parametrizations underestimate the strong LLJ at 100 m above the ground. The intermittent turbulence for this night allows the upper portion of the boundary layer to decouple from surface friction, and then accelerates the flow above the atmospheric surface layer (Stull 1988; Banta et al. 2002). Thus, to accurately predict the strong LLJ at night, the model should reasonably reproduce the intermittent turbulence. However, all experiments overestimate u_*, and are incapable of simulating the decoupling. Thus, the acceleration of the flow cannot occur.

As expected from the large diffusivities and their vertical variations (cf. Fig. 6d, e), the YSU experiment shows too strong mixing below 250 m for all θ, q_v, and U. In particular, the momentum mixing is excessively strong such that the simulated wind speed is too low below 400 m, and the LLJ at 100 m is not apparent (Fig. 8c). Destroying the vertical gradient of wind speed in the YSU PBL scheme is a systematic deficiency of the scheme (Storm et al. 2009). For wind direction, all PBL schemes are capable of predicting considerable wind turning in the SBL, while the directional wind shear is slightly overestimated below 250 m (Fig. 8d).

In summary, it is concluded that the scheme with non-local mixing and the entrainment flux proportional to the surface flux is favourable for reproducing the weakly stable temperature profile in the CBL. In the SBL, the cutting edge turbulence-closure schemes have common deficiencies in their performance, but the local TKE closure schemes perform better than the two non-local approaches. The ACM experiment shows strongly mixed profiles above the boundary-layer top, while the excessive momentum mixing near the surface appears in the YSU experiment.

5.3 Sensitivity to Surface-Layer Formulations

Through additional four experiments using the BouLac PBL parametrization and four different surface-layer schemes (i.e., the BL_YSU, BL_MYJ, BL_QNSE, and BL_ACM2 experiments) (cf. Table 1b), we aim to answer two questions. First, how much do surface-layer schemes contribute to the characteristic performance of PBL parametrizations? Secondly, how much is the variability among PBL parametrizations attributed to surface-layer schemes?

The time series of surface variables are compared in Fig. 9. The standard deviation (STD) of the surface variables of PBL and surface-layer sensitivity experiments is computed (Table 2). It is apparent that surface temperatures are almost fully characterized by surface-layer formulations, except for the nighttime temperatures from the ACM2 and BL_ACM2 experiments that use the PX surface-layer scheme (cp. Figs. 4a and 9a). The standard deviation (STD) of the four surface-layer sensitivity experiments is also larger than the STD of the five PBL

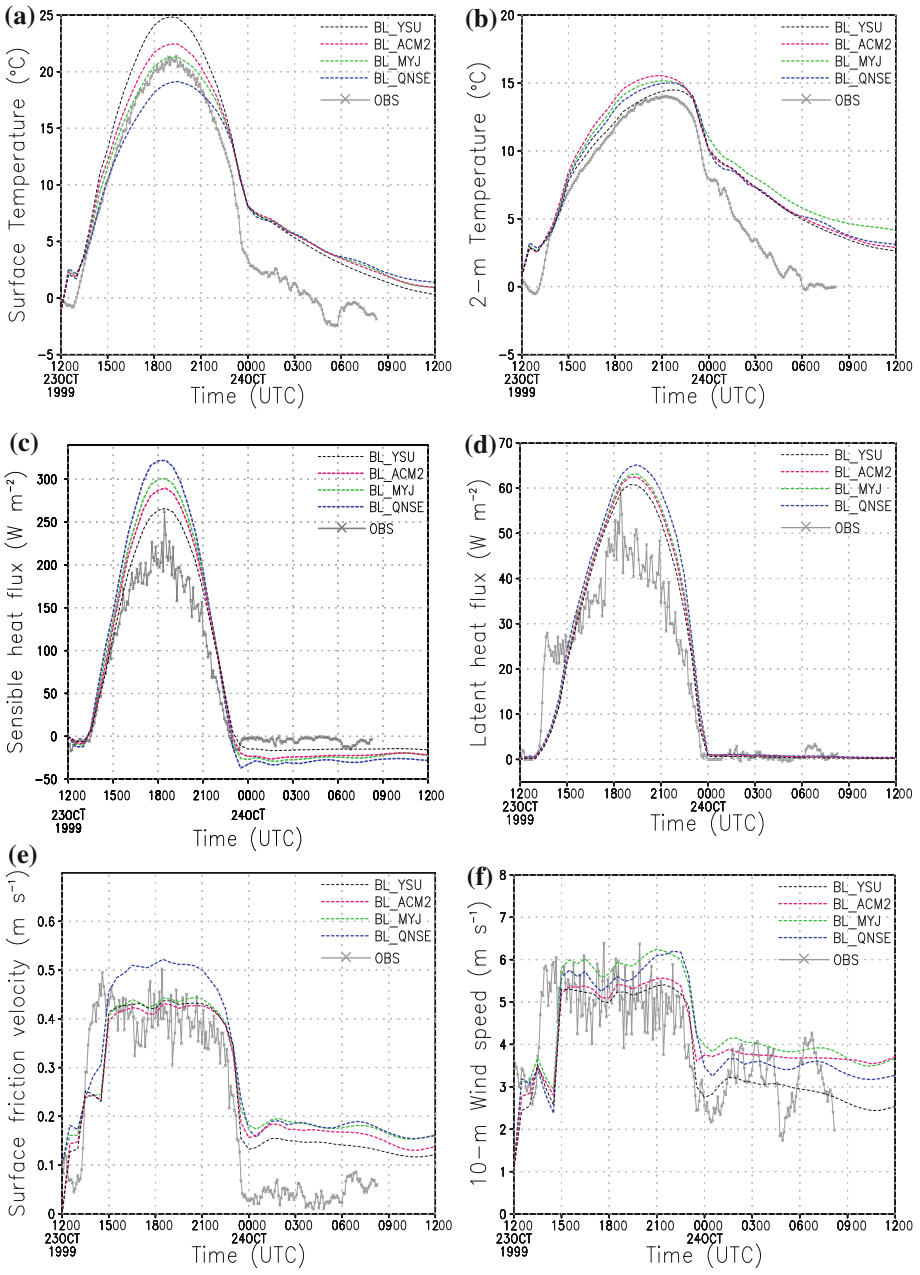

Fig. 9 Time series of simulated **a** surface temperature (°C), **b** 2-m temperature (°C), **c** sensible heat flux ($W\,m^{-2}$), **d** latent heat flux ($W\,m^{-2}$), **e** surface friction velocity ($m\,s^{-1}$), and **f** 10-m wind speed ($m\,s^{-1}$) with corresponding observations (*grey lines with cross marks*). The simulated results are from the BL_YSU (*black short dashed*), BL_ACM2 (*red short dashed*), BL_MYJ (*green short dashed*), and BL_QNSE (*blue short dashed*) experiments

Table 2 Standard deviations (STD) of the simulated surface temperature, 2-m temperature, surface sensible heat flux, latent heat flux, surface friction velocity, and 10-m wind speed of five PBL intercomparison experiments (YSU, ACM2, MYJ, QNSE, and BouLac) and of four surface-layer sensitivity experiments (BL_YSU, BL_ACM2, BL_MYJ, and BL_QNSE) for both (a) convective regime and (b) stable regime

	T_{SFC} (K)	T_2 (K)	H ($\mathrm{W\,m^{-2}}$)	LH ($\mathrm{W\,m^{-2}}$)	u_* ($\mathrm{m\,s^{-1}}$)	U_{10} ($\mathrm{m\,s^{-1}}$)
(a) Convective regime						
STD of PBL intercomparison experiments	1.02	0.49	9.54	1.02	0.01	0.27
STD of surface-layer sensitivity experiments	1.16	0.36	11.21	1.32	0.02	0.29
(b) Stable regime						
STD of PBL intercomparison experiments	0.20	0.39	4.25	0.11	0.01	0.41
STD of surface-layer sensitivity experiments	0.24	0.39	4.95	0.12	0.01	0.38

Larger values are underlined

intercomparison experiments (Table 2). This implies that the surface-temperature variability of PBL intercomparison experiments (i.e., in Sect. 5.1) is largely attributed to differences in the surface-layer scheme that is tied to each PBL parametrization, rather than to the PBL parametrization itself. The behaviour of the 2-m temperatures is also dependent on the surface-layer scheme, again except for the nighttime temperatures from the ACM2 and BL_ACM2 experiments (cp. Figs. 4b and 9b). However, the STD of the surface-layer sensitivity experiments is smaller than (comparable to) that of the PBL intercomparison experiments in the convective (stable) regime; this suggests that the variability of the 2-m temperatures arises from both surface-layer and PBL schemes. The sensible heat flux is nearly dependent only on the surface-layer scheme in both convective and stable regimes (cp. Figs. 4c and 9c), and the STD even increases in the surface-layer sensitivity experiments (Table 2). The sensitivity of the latent heat flux is similar to that of the sensible heat flux, except for the BL_ACM2 experiment (cp. Figs. 4d and 9d).

The simulated surface friction velocity (Fig. 9e) and 10-m wind speed (Fig. 9f) show quite different sensitivity from the temperatures and fluxes. The friction velocities converge to the BL_MYJ (BouLac) experiment excluding the BL_QNSE experiment in the convective regime, indicating that u_* is more dependent on the vertical diffusion schemes than on the surface-layer schemes. However, due to the BL_QNSE experiment, which is very different from the other three experiments, the STD of the surface-layer sensitivity experiments is larger. It is noted that the MM5, PX, and Eta surface-layer parametrizations use similar empirical stability functions (ψ_m and ψ_h) for calculating exchange coefficients and surface fluxes. However in the case of the QNSE, the stability functions are derived from the QNSE theory consistent with the QNSE PBL scheme (Galperin and Sukoriansky 2010), and the drag coefficients from the theory are slightly larger than those from the empirical functions (B. Galperin, personal communication, 2010). In the stable regime, the fluctuations of u_* of the four surface-layer sensitivity experiments become similar (cp. Figs. 4e and 9e). The 10-m wind speed shows similar sensitivity to that of the surface friction velocity (Fig. 9f).

Under the first GABLS intercomparison project for a stably stratified atmospheric boundary layer, Cuxart et al. (2006) mentioned that the European Centre for Medium-Range Weather Forecasts SCM with low vertical resolution is largely affected by changes in the surface-layer formulation, while the Japan Meteorological Agency (JMA) SCM at high resolution is not so sensitive to the changes. They determined that, if the vertical resolution is higher than the Obukhov length, as for the JMA SCM, the surface-layer parametrization does

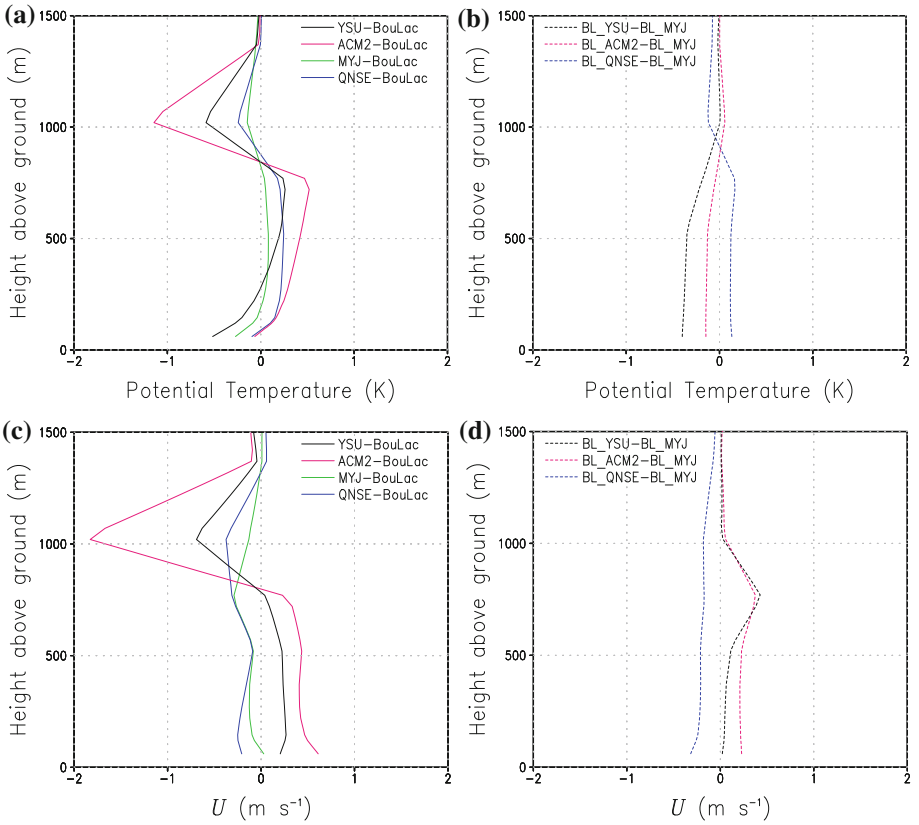

Fig. 10 Vertical profile differences of PBL intercomparison experiments from the BouLac experiment (*left panels*) and differences of surface-layer sensitivity experiments from the BL_MYJ experiment (*right panels*) in **a**, **b** potential temperature (K), and **c**, **d** wind speed ($\mathrm{m\,s^{-1}}$) at 1900 UTC 23 October (1400 LST 23 October)

not seem so important. It is noted that the lowest model-layer height is 40 m, and about half of the boundary layer is below this height at the nighttime (cf. Fig. 5); the strong dependency of the simulated surface variables to surface-layer schemes in the stable regime is inevitable under this vertical resolution. However, these results are restricted to the current grid size, and are changeable given the higher resolution near the surface.

Compared to the surface variables, vertical profiles are less dependent on surface-layer schemes. Figure 10 shows differences of the vertical profile of the BouLac experiment from other four PBL intercomparison experiments (left panels), and differences of the vertical profile of the BL_MYJ experiment from other three surface-layer sensitivity experiments (right panels) at 1900 UTC 23 October. The former includes the effects of PBL and surface-layer parametrizations as well as non-linear interactions between the two physics schemes, while the latter shows the effects of surface-layer schemes. For the potential temperature, surface-layer schemes only contribute to the near-surface variability and then the mixed-layer mean properties (cp. Fig. 10a, b). In other words, the PBL parametrizations are responsible for the shape of the vertical profiles and then for the variability of the vertical profiles. This interpretation is also applied to the wind speed (cp. Fig. 10c, d). Vapour mixing ratio profiles

show almost no differences among the four surface-layer sensitivity experiments, implying the effects of the surface-layer formulations are insignificant (not shown). At nighttime, thermal fluxes from the surface disappear, and so the surface-layer schemes have less impact on θ profiles than at the daytime, and the schemes only contribute to the near-surface profile for wind speed (figures not shown).

6 Concluding Remarks

We compared characteristics of five PBL parametrizations in the WRF numerical model: the YSU, ACM2, MYJ, QNSE, and BouLac PBL parametrizations. Through the intercomparison, we highlighted the advantages and disadvantages of each scheme, focusing on the prediction of near-surface and PBL properties. Simulations with the five PBL schemes were conducted for one selected day from the CASES-99 field experiment, and results from the numerical simulations with the 3-km resolution were analysed.

Intercomparison results revealed that discrepancies of thermodynamic surface variables—the surface temperature, 2-m temperature, sensible and latent heat fluxes—among the five PBL schemes are large at daytime, and averages of the five experiments are closer to tower measurements than at nighttime; the variables converge at nighttime, but their values are much higher than those observed. On the other hand, surface friction velocity and 10-m wind speed are more divergent at the nighttime, and biases from observations are also larger than at the daytime. From these results, it was concluded that the representation of surface variables is still uncertain even with state-of-the-art PBL schemes, especially under stable conditions. Regarding diffusivity profiles, the diffusivities are different only in terms of their magnitude for convective conditions, while for stable conditions they are different in terms of both magnitude and maximum-diffusivity height. In regard to PBL structures, a non-local scheme with the entrainment flux proportional to the surface flux is favourable under unstable conditions. Under stable conditions, there is no PBL scheme that satisfactorily simulates the SBL and upper inversion. However, the local TKE closure schemes perform better than the first-order approaches.

We also assessed the relative contributions of surface-layer schemes to the typical features of each PBL parametrization, noting that the surface-layer formulations differ according to PBL schemes used. It was found that thermodynamic surface variables are more strongly influenced by the surface-layer schemes than by the vertical mixing algorithms of PBL parametrizations, in both convective and stable regimes. However, the near-surface momentum depends on the vertical diffusion schemes in the unstable regime. Compared to the surface variables, vertical profiles are less dependent on the surface-layer schemes. The surface-layer parametrizations only contribute to near-surface variability in both unstable and stable regimes, whereas the shapes of the profiles are determined by the PBL mixing algorithms.

In the recent study of Nolan et al. (2009), it was shown that a modification in surface-layer formulations that considers a more recently formulated ocean roughness length improves their hurricane simulations with both the YSU and MYJ schemes. This implies that there are possibly many error sources in the surface-layer schemes, and these errors can affect the performance of PBL parametrizations.

Acknowledgments This research was funded by the Korea Meteorological Administration Research and Development Program under grant CATER_2007_4406. The use of the computing system by grant No. KSC 2009-G2-0002 from Korea Institute of Science and Technology Information (KISTI) is also greatly appreciated. This work was also supported by the Brain Korea 21 project in 2010. We would like to express our gratitude to

Jimy Dudhia for his valuable comments in the early stages of our study. We also appreciate Boris Galperin's constructive comments on the QNSE scheme. We thank the three anonymous reviewers and the editor for helping to improve the final version of the manuscript.

References

Banta RM, Newsom RK, Lundquist JK, Pichugina YL, Coulter RL, Mahrt L (2002) Nocturnal low-level jet characteristics over Kansas during CASES-99. Boundary-Layer Meteorol 105:221–252

Bougeault P, Lacarrére P (1989) Parameterization of orography-induced turbulence in a mesobeta-scale model. Mon Weather Rev 117:1872–1890

Braun SA, Tao W-K (2000) Sensitivity of high-resolution simulations of hurricane Bob (1991) to planetary boundary layer parameterizations. Mon Weather Rev 128:3941–3961

Chen F, Dudhia J (2001) Coupling an advanced land-surface/hydrology model with the Penn State/NCAR MM5 modeling system. Part I: model description and implementation. Mon Weather Rev 129:569–585

Chou M-D, Suarez MJ (1999) A solar radiation parameterization for atmospheric studies. Technical report series on Global modeling and data assimilation 104606, vol 15, 38 pp

Cuxart J, Holtslag AAM, Beare RJ, Bazile E, Beljaars A, Cheng A, Conangla L, Ek M, Freedman F, Hamdi R, Kerstein A, Kitagawa H, Lenderink G, Lewellen D, Mailhot J, Mauritsen T, Perov V, Schayes G, Steeneveld G-J, Svensson G, Taylor P, Weng W, Wunsch S, Xu K-M (2006) Single-column model intercomparison for a stably stratified atmospheric boundary layer. Boundary-Layer Meteorol 118:273–303

Ek MB, Mitchell KE, Lin Y, Rogers E, Grunmann P, Koren V, Gayno G, Tarpley JD (2003) Implementation of Noah land surface model advances in the National Centers for Environmental Prediction operational mesoscale Eta model. J Geophys Res 108:D22. doi:10.1029/2002JD003296

Galperin B, Sukoriansky S (2010) Progress in turbulence parameterization for geophysical flows. In: The 3rd international workshop on Next-generation NWP models: bridging parameterization, explicit clouds, and large eddies. Seoul, Korea, 5.4. http://nml.yonsei.ac.kr/20100829/content/agenda.html

Holt T, Raman S (1988) A review and comparative evaluation of multilevel boundary layer parameterizations for first-order and turbulent kinetic energy closure models. Rev Geophys 26:761–780

Holtslag AAM, Boville BA (1993) Local versus nonlocal boundary-layer diffusion in a global climate model. J Clim 6:1825–1842

Hong S-Y (2010) A new stable boundary-layer mixing scheme and its impact on the simulated East Asian summer monsoon. Q J Roy Meteorol Soc 136:1481–1496

Hong S-Y, Pan H-L (1996) Nonlocal boundary layer vertical diffusion in a medium-range forecast model. Mon Weather Rev 124:2322–2339

Hong S-Y, Noh Y, Dudhia J (2006) A new vertical diffusion package with an explicit treatment of entrainment processes. Mon Weather Rev 134:2318–2341

Janjić ZA (1990) The step-mountain coordinate: physics package. Mon Weather Rev 118:1429–1443

Kim Y-J, Hong S-Y (2009) Interaction between the orography-induced gravity wave drag and boundary layer processes in a global atmospheric model. Geophys Res Lett 36:L12809. doi:10.1029/2008GR037146

Li X, Pu Z (2008) Sensitivity of numerical simulation of early rapid intensification of hurricane Emily (2005) to cloud microphysical and planetary boundary layer parameterizations. Mon Weather Rev 136:4819–4838

Mlawer EJ, Taubman SJ, Brown PD, Iacono MJ, Clough SA (1997) Radiative transfer for inhomogeneous atmosphere: RRTM, a validated correlated-k model for the long-wave. J Geophys Res 120:16663–16682

Musson-Genon L (1995) Comparison of different simple turbulence closures with a one-dimensional boundary layer model. Mon Weather Rev 123:163–180

Noh Y, Cheon W-G, Hong S-Y (2003) Improvement of the K-profile model for the planetary boundary layer based on large eddy simulation data. Boundary-Layer Meteorol 107:401–427

Nolan DS, Zhang JA, Stern DP (2009) Evaluation of planetary boundary layer parameterizations in tropical cyclones by comparison of in situ observations and high-resolution simulations of hurricane Isabel (2003). Part I: initialization, maximum winds, and the outer-core boundary layer. Mon Weather Rev 137:3651–3674

Pleim JE (2006) A simple, efficient solution of flux–profile relationships in the atmospheric surface layer. J Appl Meteorol Clim 45:341–347

Pleim JE (2007a) A combined local and nonlocal closure model for the atmospheric boundary layer. Part I: model description and testing. J Appl Meteorol Clim 46:1383–1395

Pleim JE (2007b) A combined local and nonlocal closure model for the atmospheric boundary layer. Part II: application and evaluation in a mesoscale meteorological model. J Appl Meteorol Clim 46:1396–1409

Poulos GS, Blumen W, Fritts DC, Lundquist JK, Sun J, Burns SP, Nappo C, Banta R, Newsom R, Cuxart J, Terradellas E, Balsley B, Jensen M (2002) CASES-99: a comprehensive investigation of the stable nocturnal boundary layer. Bull Am Meteorol Soc 83:555–581

Sharan M, Gopalakrishnan SG (1997) Comparative evaluation of eddy exchange coefficients for strong and weak wind stable boundary layer modeling. J Appl Meteorol 36:545–559

Skamarock WC, Klemp JB, Dudhia J, Gill DO, Barker DM, Duda MG, Huang X-Y, Wang W, Powers JG (2008) A description of the advanced research WRF version 3. NCAR TECHNICAL NOTE, NCAR/TN-475+STR, 113 pp

Steeneveld GJ, Mauritsen T, DeBruijn EIF, DeArellano JV-G, Svensson G, Holtslag AAM (2008) Evaluation of limited-area models for the representation of the diurnal cycle and contrasting nights in CASES-99. J Appl Meteorol Clim 47:869–887

Storm B, Dudhia J, Basu S, Swift A, Giammanco I (2009) Evaluation of the Weather Research and Forecasting model on forecasting low-level jets: implication for wind energy. Wind Energy 12:81–90

Stull RB (1988) An introduction to boundary layer meteorology. Kluwer, The Netherlands, 666 pp

Sukoriansky S, Galperin B, Perov V (2005) Application of a new spectral theory of stable stratified turbulence to the atmospheric boundary layer over sea ice. Boundary-Layer Meteorol 117:231–257

Svensson G, Holtslag AAM (2006) Single column modeling of the diurnal cycle based on CASES99 data-GABLS second intercomparison project. In: 17th symposium on Boundary layers and turbulence. American Meteorological Society, San Diego, CA, Paper 8.1

van de Wiel BJH, Moene AF, Hartogensis OK, de Bruin HAR, Holtslag AAM (2003) Intermittent turbulence in the stable boundary layer over land. Part III: a classification for observations during CASES-99. J Atmos Sci 60:2509–2522

Zhang D, Anthes RA (1982) A high-resolution model of the planetary boundary layer—sensitivity tests and comparison with SESAME-79 data. J Appl Meteorol 21:1594–1609